Hue University Journal of Science: Natural Science
Vol. 132, No. 1D, 55–62, 2023

pISSN 1859-1388
eISSN 2615-9678

Facile synthesis of 3D Fe_2O_3 nanostructures: sponge-like cube shape and bird nest-like architecture

Tran Quy Phuong[1], Ho Van Minh Hai[1], Tran Thai Hoa[1], Nguyen Duc Cuong[1,2]*

[1] University of Sciences, Hue University, 77 Nguyen Hue, Hue, Viet Nam
[2] School of Hospitality and Tourism, Hue University, 22 Lam Hoang, Hue, Viet Nam

* Correspondence to Nguyen Duc Cuong <nguyenduccuong@hueuni.edu.vn>

(*Received: 16 December 2022; Revised: 27 March 2023; Accepted: 13 April 2023*)

Abstract. The hierarchical nanostructures (3D) with their large specific surface area and abundant pores usually possess unique physical and chemical properties for various important applications. In this report, we have introduced simple and scalable routes to successfully synthesize 3D iron oxide nanostructures, including porous cubes and bird nest-like architecture. The 3D sponge-like Fe_2O_3 nanocubes were formed by an annealing process of perfect Prussian Blue (PB) microcubes, which were built from small nanoparticles linked together. Whereas, the 3D bird nest-like Fe_2O_3 nanostructures were formed by the transformation of C@FeOOH nanoflower precursors, which were constructed by primary nanorods. The results indicated that the obtained materials show monodispersity, uniform morphology, ultra-porosity and extremely high specific surface area. With unique characteristics, the 3D Fe_2O_3 nanostructures could be potential candidates for various important fields such as catalysts, absorption and gas sensors.

Keywords: 3D nanostructure, sponge-like nanocube, bird nest-like architecture, iron oxide

1 Introduction

The 3D porous nanostructures are built by an interconnected network of pores, which are fantastic materials for many important areas [1]. These unique architectures usually possess high specific surface area, abundant porosity and enhancement of adsorption/reaction sites, which may originate from the combination of macroscopic properties of the total system with nanoscopic scale [2]. Semiconducting metal oxide is one type of 3D porous material that has attracted a lot of interest because it combines the unique intrinsic properties of metal oxide semiconductors with the benefits of porous system derived from the high surface area and large pore volume [3], which are useful for catalysts, absorption and sensors [4]. However, it is very difficult to synthesize 3D porous metal oxide nanostructures by facile hydrothermal methods.

Due to its appealing chemical and physical properties, nontoxicity, and low cost [5], iron oxide nanostructure is a significant class of materials that have been investigated for use in several fields, including catalysis [6], magnetic materials [7], lithium-ion batteries [8], gas sensors [9], and bio-sensing and medical applications. Among various iron oxide nanostructures, the porous nanostructures frequently improve their properties in a variety of applications. For example, Kim et al. reported that the Fe_2O_3 hollow spheres showed significantly enhanced C_2H_5OH sensing properties in comparison to their counterparts, such as Fe_2O_3 spheres with solid inner structures and agglomerated nanoparticles [6]. The porous spindle-like α-Fe_2O_3 nanoparticles

with high surface area and large pore volume were used as anode materials for Lithium-ion batteries, which showed outstanding electrochemical performance [8]. The porous α-Fe_2O_3 quasi-single crystal hierarchical tubule-based sensor exhibited high-performance ppb-level H_2S gas, which was more than twice that of reported α-Fe_2O_3 sensing materials [9]. The porous Fe_2O_3 nanorods were used as a catalyst to photodegrade Rhodamine B, methylene blue, methyl orange, p-nitrophenol, and eosin B, which exhibited higher catalytic activities due to their large surface areas and porous nanostructures in comparison with the commercial Fe_2O_3 powder [10]. As a result, the design of novel porous Fe_2O_3 nanostructures with high porosity is considered one of the most important strategies to explore new applications.

Various synthetic routes have been developed to create highly porous metal oxide nanostructures. Among them, metal-organic framework (MOF), which is constructed by metal ions and poly-functional organic ligands to form an outstanding structure with extremely specific surface area and high porosity, has been considered a promising route for the fabrication of ultra-porous metal oxide nanostructures [11]. Gao et al. successfully synthesized α-Fe_2O_3 porous nanorods by thermolysis of MIL-88A at 500 ^oC. The obtained α-Fe_2O_3 nanorods preserved well a uniform morphology with porous internal structures [12]. The Fe-MIL-88A was also used as a potential template for converting to γ-Fe_2O_3 nanoparticles embedded in porous carbon via one-step simple pyrolysis at 500 ^oC [13]. A controlled self-etching reaction was employed by Hu et al. to fabricate Prussian Blue (PB) hollow nanoparticles, which were then used as a potential precursor to creating superparamagnetic nanoporous iron oxides with hollow internal cavities by utilizing a thermal decomposition process [7]. By heating uniform PB microcubes in air at different temperatures, Zhang et al. [14] synthesized hierarchical Fe_2O_3 microboxes with various shell structures. The porous Fe_2O_3 nanocubes composed of fine nanoparticles were fabricated by the decomposition of PB at high temperatures [15]. Besides, several attempts have also applied carbonaceous sphere templates to synthesize 3D highly porous iron oxide nanostructures such as $\boldsymbol{\alpha}$-Fe_2O_3 double-layer hollow spheres [16], porous $\boldsymbol{\alpha}$ -Fe_2O_3 hollow microsphere [17], multi-shelled α-Fe_2O_3 microspheres [18] and so on. Therefore, using Fe-MOF and carbonaceous spheres as templates is a very important strategy to prepare ultra-porous 3D Fe_2O_3 structures.

In this report, uniform PB microcubes and carbon microspheres were used as potential templates for the fabrication of 3D porous Fe_2O_3 nanostructures. The 3D sponge-like γ-Fe_2O_3 nanocubes were formed by the assembly of numerous fine nanoparticles through the simultaneous oxidative decomposition of PB. The 3D bird nest-like Fe_2O_3 nanoarchitectures were synthesized by the hydrothermal method using carbon microspherical templates, which were built by the assembly of primary nanorods.

2 Experimental

2.1 Synthesis of 3D sponge-like iron oxide microcubes

The following chemicals were purchased from Sigma–Aldrich and utilized without additional purification: Potassium hexacyanoferrate(II) ($K_4Fe(CN)_6{\cdot}3H_2O$), Polyvinyl Pyrrolidone (PVP). The 3D ultra-porous α-Fe_2O_3 nanocubes were easily prepared by directly annealing the Prussian blue (PB). For the manufacture of the PB nanocube precursor, 0.11 g of $K_4Fe(CN)_6{\cdot}3H_2O$ and 3.8 g of polyvineypirrolydone (PVP, K30, MW ~ 40000) were dissolved in 50 mL of HCl 0.1 M aqueous solution by magnetic stirring for 30

pISSN 1859-1388
eISSN 2615-9678

min to form a homogeneous yellow solution, which was transferred into a 100 mL Teflon-lined autoclave, and then aged for 24 h at 90 °C. The obtained PB blue crystals (Prussian blue) were collected, repeatedly washed with water and ethanol, and then dried at 80 °C for 24 h. The PB nanocubes were annealed for 3 h at 500 °C to form 3D sponge-like γ-Fe_2O_3 nanocubes.

2.2 Synthesis of 3D bird nest-like Fe_2O_3 nanostructures

The hydrothermal approach was used to design the 3D nest-like α-Fe_2O_3 nanoarchitectures utilizing carbonaceous spherical templates. We started by getting the carbonaceous sphere ready. In a typical procedure, 4 g of glucose (Sigma–Aldrich) was added into 40 mL of deionized water to obtain a homogeneous solution. This solution was then transferred into a Teflon-lined autoclave (100 mL). The mixture was aged for 4 h at 140 °C and then for 4 h at 180 °C. The carbonaceous sphere was collected, repeatedly washed with deionized water and ethanol, and then dried for 24 h at 60 °C. To synthesize C@FeOOH microspheres, 0.08 g of as-prepared carbonaceous microspheres were ultrasonically dispersed in 50 mL of deionized water. After that, 2 mmol of $FeSO_4{\cdot}7H_2O$ and 0.3 g of CH_3COONa were added to this suspension. At room temperature, the mixture was vigorously stirred for 24 h. The precipitation was separated and purified multiple times with water and ethanol. The obtained material was dried for 10 h at 80 °C. The 3D bird nest-like Fe_2O_3 nanoarchitectures were produced by calcining the resulting composites at 600 °C for 2 h.

2.3 Material characterizations

X-ray diffraction patterns (XRD) were measured on a Bruker D8 Advance x-ray diffractometer with a Cu-Kα line source (λ ~ 1.5406 Å). Scanning Electron Microscopy (SEM) was performed on JSM-5300LV instrument. Transmission electron microscopy (TEM) and high-resolution TEM (HRTEM) and selected area electron diffraction (SAED) were conducted on JEOL JEM 1230. N_2 adsorption/desorption isotherm (Micromeritics Tristar 3030) was used to determine the specific surface area and pore size distribution of samples using the Brunauer–Emmett–Teller (BET) equation and the Barret–Joyner–Halender (BJH) method, respectively.

3 Results and discussions

3.1 Hierarchical sponge-like Fe_2O_3 nanocubes

The morphology of the PB precursor and the sponge-like Fe_2O_3 nanocube is analyzed by SEM and TEM techniques, as shown in figure 1. For the PB precursor, the SEM image (1a) indicates that the as-synthesized PB has a typical cubic shape with smooth surfaces that is uniform and well dispersed. The edge length of the PB cubes is in the range of 200-300 nm. TEM image (figure 1b) provides additional details about the perfect cubical structure of PBs. Similar to the SEM result, the TEM image likewise shows cubes with sharp edges and corners. After being annealed at 500 °C for 3 h in air, the calcined material still retains the cubic shape of PB precursor. However, the morphology reveals a sponge-like cube shape with an extremely rough surface (figure 1c). The sponge cubes have a unique 3D porous network, as seen in the TEM image (figure 1d), which is made up of interconnected pores and nanoparticles that arise from the oxidative decomposition of $Fe_4[Fe(CN)_6]_3$ [19].

The phase of sponge-like Fe_2O_3 nanocubes was determined by SAED and HRTEM, as illustrated in figure 2. All concentric diffraction rings that may relate to the diffraction (220), (311), (400), (422), (511) and (440) planes of γ-Fe_2O_3 are assigned by the SAED result (figure 2a). In addition, the HRTEM in figure 2b clearly presents

lattice fringes with a spacing of 0.25 nm, indicating the (311) planar spaces of γ-Fe_2O_3 nanostructure. XRD patterns were also used to determine the crystal structures of sponge-like γ-Fe_2O_3 nanocubes. The XRD pattern of the sample in figure 3a closely matches cubic spinal γ-Fe_2O_3 (JCPDS card no. 39-1346). The XRD curve shows no peak for any other phases, which demonstrates that the PB precursor is completely transformed into maghemite after the annealing process. The XRD of the sponge-like γ-Fe_2O_3 nanocubes shows a weak intensity and broad reflection, which is consistent with their assembly of many small nanoparticles [20].

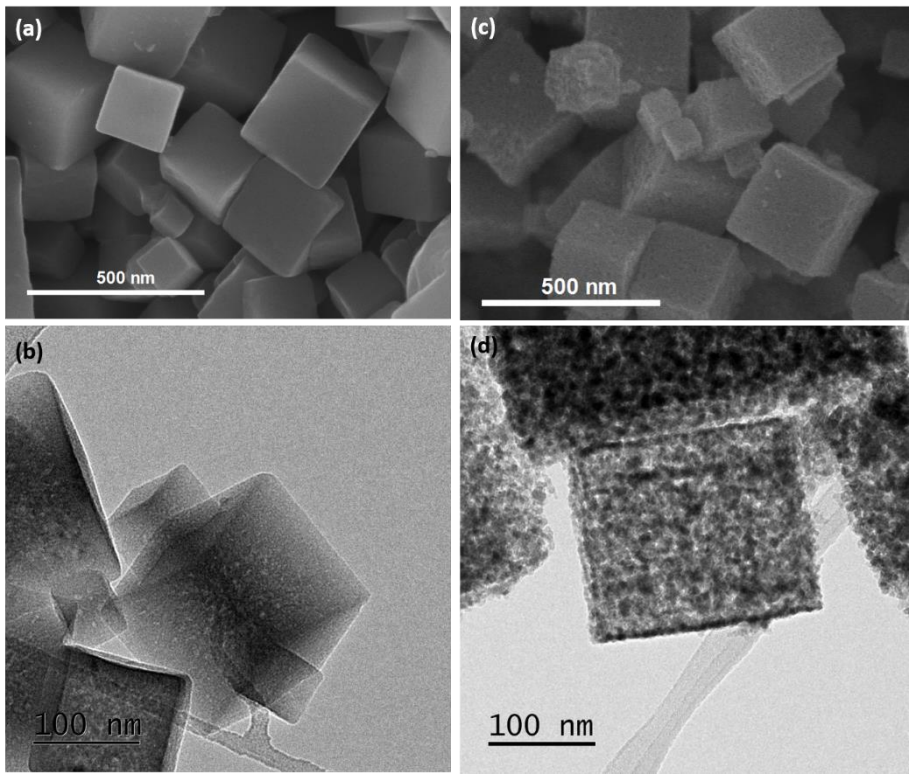

Fig. 1. The SEM (a) and TEM (b) images of PB, and SEM (c) and TEM (d) images of 3D sponge-like γ-Fe_2O_3 nanocube

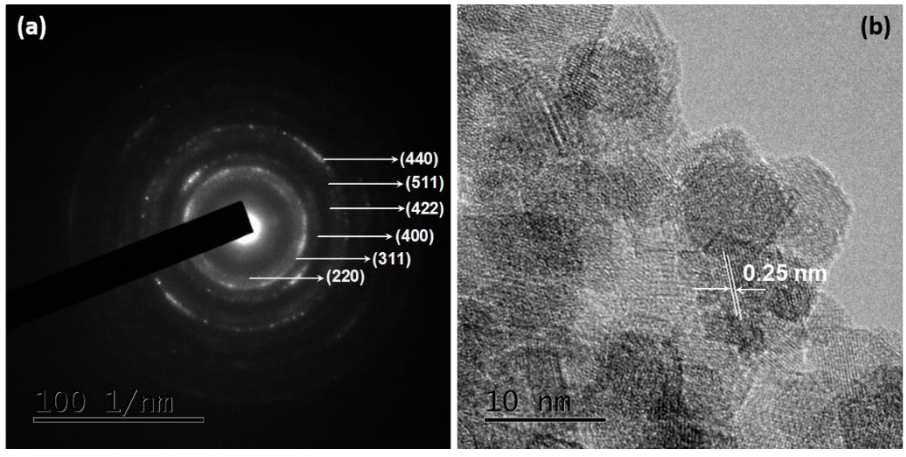

Fig. 2. The SAED (a) and HRTEM (b) of 3D sponge-like γ-Fe_2O_3 nanocube

pISSN 1859-1388
eISSN 2615-9678

The N_2 adsorption/desorption isotherm, as illustrated in figure 3b, confirms further the porous structure of sponge-like maghemite nanocubes. The nitrogen adsorption-desorption isotherm can be classified as a type IV isotherm, which characterizes the existence of mesoporous structures [21]. Besides, the hysteresis loops can be classified as type H3, implying the isotherm occurs with aggregates of nanoparticles giving rise to slit-shaped pores [22]. The obtained material has a high BET specific surface area of 95 m_2 g^{-1}, and its BHJ pore size distribution plot is centered at mesopores. The as-synthesized 3D sponge-like γ-Fe_2O_3 nanocubes with large surface area and abundant mesopores may have unique chemical and physical properties for critical applications.

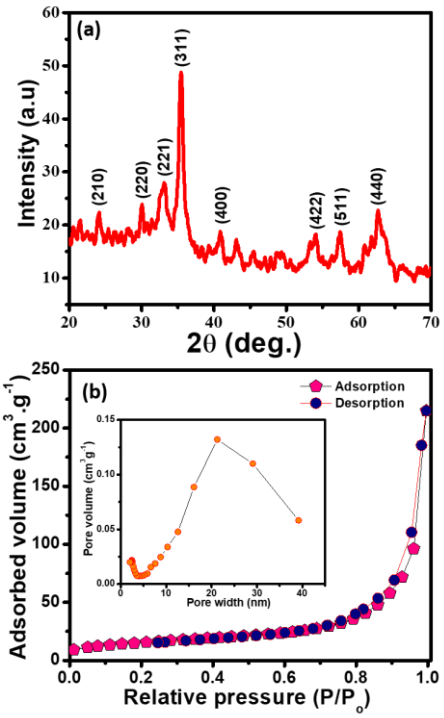

Fig. 3. The XRD pattern (a) and nitrogen adsorption/desorption isotherm (b) of 3D sponge-like γ-Fe_2O_3 nanocube

3.2 Hierarchical bird nest-like nanoarchitecture

The mechanistic formation of carbon microspheres by the hydrothermal process of glucose involves glucose polymerization at low temperatures (< 180 °C) followed by carbonization at a higher temperature, with polymer concentration playing an important role in nucleation [23]. Besides, nucleation, which occurs usually in a short period and is separated from the growth process, plays a key role in obtaining uniform nanoparticles via hydrothermal routes [24]. On this basis, in order to prepare uniform carbon microsphere templates, we used a two-stage hydrothermal route of glucose at 140 °C and 180 °C. The supersaturation solution of polymers was formed at 140 °C, and then the burst nucleation and growth occurred at 180 °C. SEM images of carbon microspheres are presented in Figure 4a. As can be seen, the carbon microspheres have a diameter of around 300-400 nm and display perfect spherical morphology, smooth surface and monodispersity. The as-prepared carbon microspheres are suitable as templates for the construction of novel functional materials due to their high degree of size and shape uniformity. The SEM images of C@FeOOH microspheres are displayed in figure 4b. The C@FeOOH structures are composed of many FeOOH nanorods that grow on carbon microsphere templates. After calcination, the C@FeOOH microsphere precursors are transformed into 3D bird nest-like Fe_2O_3 nanoarchitecture (figures c-d). Figures 4 (c-d) shows SEM and TEM images that reveal the detailed morphology of 3D bird nest-like Fe_2O_3 nanoarchitecture. After the carbon microspheres are oxidized at high temperatures, the calcined sample still maintained the microspherical structure well, as seen by the SEM image in figure 4b. In the meantime, the TEM image (Figure 4d) presents that the spherical shell is made of many

Fe_2O_3 nanorods that are connected together to form 3D bird nest-like nanostructures.

The SAED pattern revealed concentric diffraction rings of α-Fe_2O_3 (figure 5a), confirming its polycrystalline nature. Furthermore, the HRTEM in figure 5b clearly shows the lattice spacing of 0.25 nm, which corresponds to the (110) plane of α-Fe_2O_3, is seen in the HRTEM in figure 5b. XRD was used to further characterize the phase purities of the calcined product (figure 6a). The XRD pattern of the calcined sample illustrates that all of the diffraction peaks closely index to the rhombohedra phase of α-Fe_2O_3 crystalline structure (JCPDS No. 33-0664). In the XRD, no peak of other phases was observed, proving the purity of the α-Fe_2O_3.

α-Fe_2O_3 nanoarchitecture with a unique 3D bird nest-like morphology is predicted to have a high porosity and a large specific surface area. By using the nitrogen adsorption/desorption isotherm, we were able to determine the porous nature of the as-synthesized nanomaterials (Figure 6b). According to the IUPAC classification, the isotherm can be classified as type IV with an H3 hysteresis loop, which indicates the presence of mesopores in the materials. The 3D bird nest-like nanoarchitecture has a high BET surface area of ~ 115 m^2g^{-1}. Using the BJH method and the desorption branch of the nitrogen isotherm, the pore diameter distribution plots of the sample (insert Figure 3d) demonstrated a bimodal pore size distribution in the mesoporous and macroporous regions.

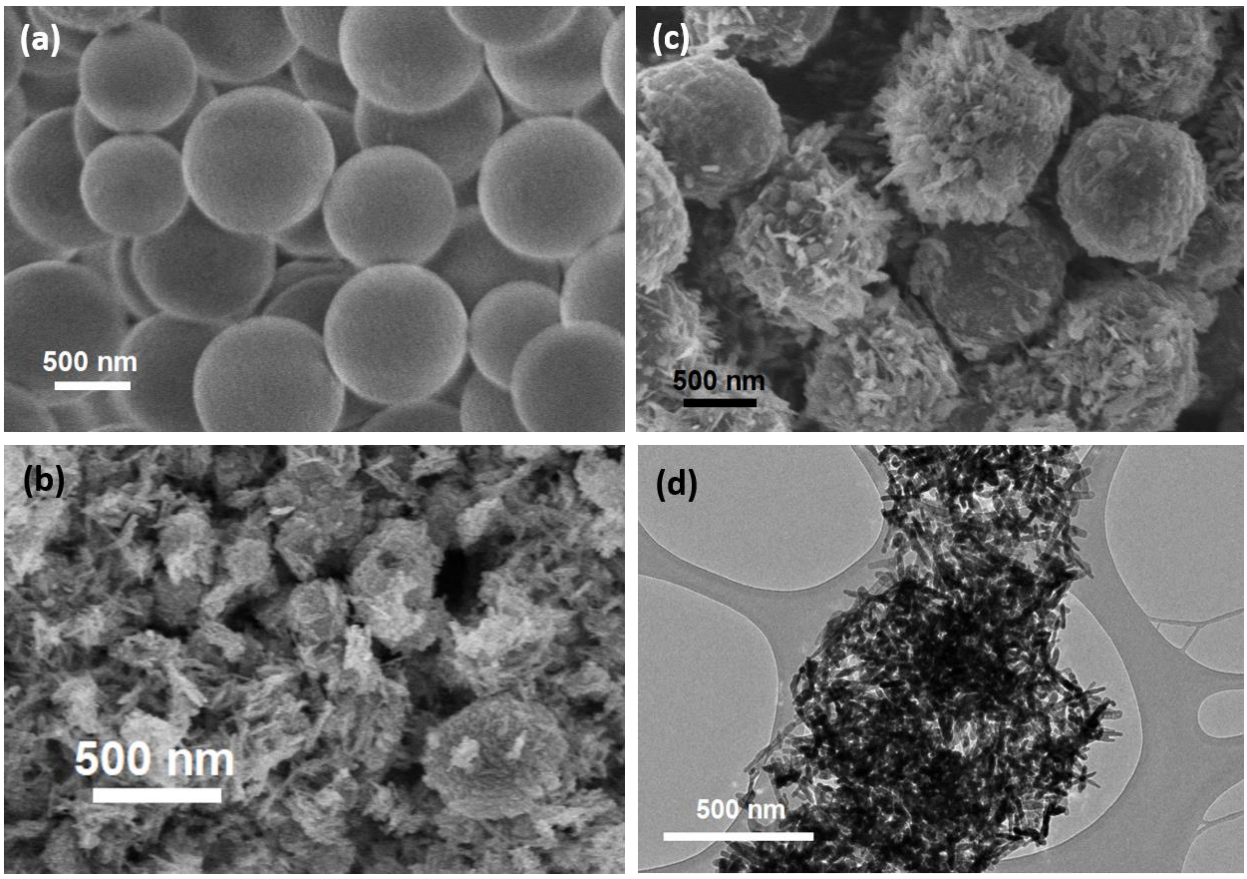

Fig. 4. The SEM (a) and TEM (b) images of carbon microspheres, and SEM (c) and TEM (d) images of 3D bird nest-like α-Fe_2O_3 nanoarchitecture

pISSN 1859-1388
eISSN 2615-9678

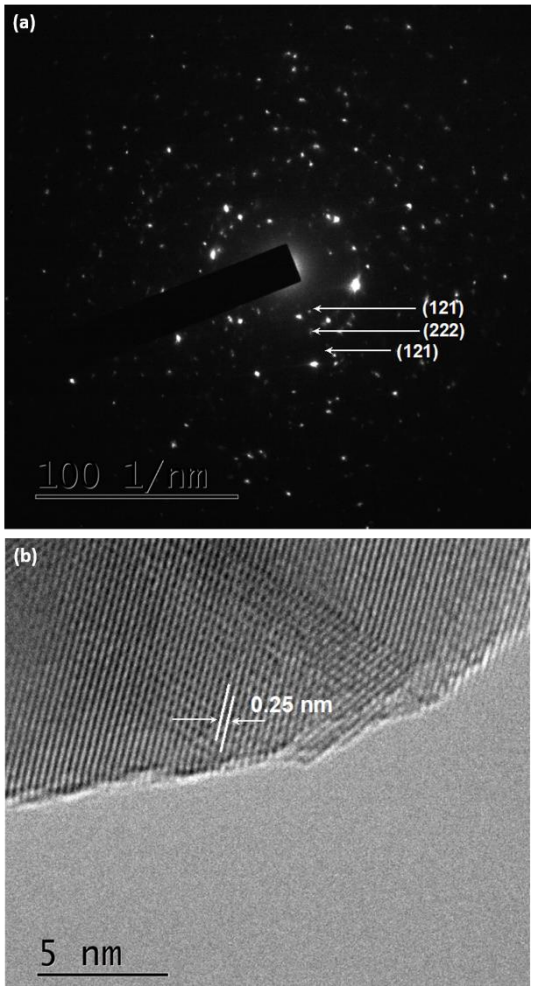

Fig. 5. The SAED (a) and HRTEM (b) of 3D bird nest-like α-Fe_2O_3 nanoarchitecture

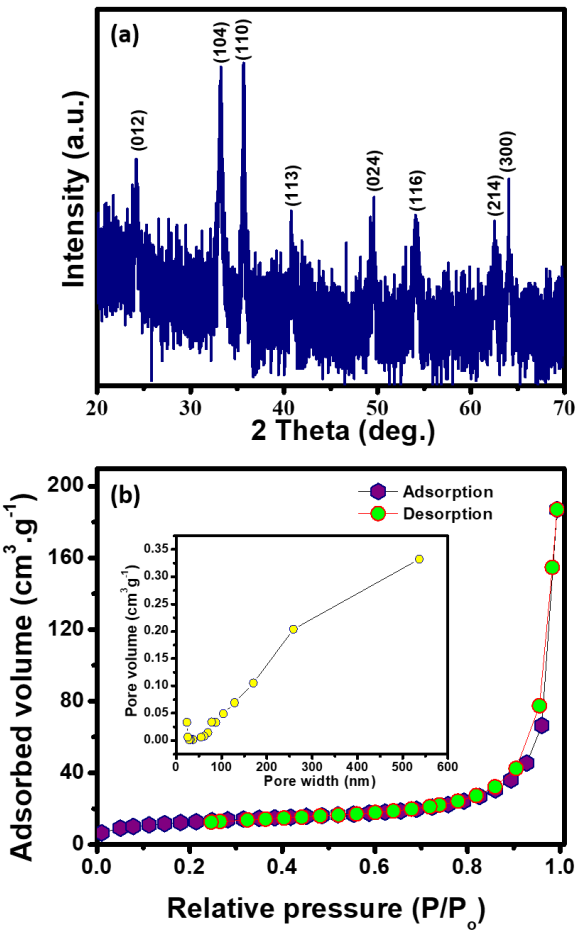

Fig. 6. The XRD pattern (a) and nitrogen adsorption/desorption isotherm (b) of 3D bird nest-like α-Fe_2O_3 nanoarchitecture

4 Conclusions

In summary, the 3D porous Fe_2O_3 nanostructures, including sponge-like γ-Fe_2O_3 nanocubes and bird nest-like α-Fe_2O_3 nanoarchitectures, were successfully synthesized by easy hydrothermal methods, using PBs and carbon microspheres as sacrificial templates, respectively. The obtained 3D iron oxide nanostructures show monodispersity, uniform morphology, ultra-porosity and extremely high specific surface area. These unique structures possess both 0D, 1D and 3D structural features, which are highly expected as potential candidates for various important fields such as catalysts, absorption, and gas sensors.

Acknowledgment

We are grateful to Vietnamese Ministry of Education and Training for funding our research under grant number B2021-DHH-14.

References

1. Nguyen TD, Tang D, Acierno FD, Michal CA, MacLachlan MJ. Biotemplated Lightweight γ-Alumina Aerogels. Chem Mater. 2018;30:1602-09.

2. Nai J, Lou XW. Hollow Structures Based on Prussian Blue and Its Analogs for Electrochemical Energy Storage and Conversion. Adv Mater. 2019;31(38):1706825.

3. Wu Q, Wu G, Wang L, Hu W, Wu H. Facile synthesis and optical properties of Prussian Blue microcubes and hollow Fe_2O_3 microboxes. Mater Sci Semicond Process. 2015; 30:476-81.

4. Wang H, Zhang X, Wang N, Li Y, Feng X, Huang Y, et al. Ultralight, scalable, and high-temperature–resilient ceramic nanofiber sponges. Sci Adv. 2017;3:1603170.

5. Cuong ND, Hoa ND, Hoa TT, Khieu DQ, Quang DT, Quang VV, Hieu NV. Nanoporous hematite nanoparticles: Synthesis and applications for benzylation of benzene and aromatic compounds. J Alloys Compd. 2014;582:83-87.

6. Kim HJ, Choi KI, Pan A, Kim ID, Kim HR, Kim KM, et al. Template-free solvothermal synthesis of hollow hematite spheres and their applications in gas sensors and Li-ion batteries. J Mater Chem. 2011;21:6549.

7. Hu M, Belik AA, Imura M, Mibu K, Tsujimoto Y, Yamauchi Y. Synthesis of Superparamagnetic Nanoporous Iron Oxide Particles with Hollow Interiors by Using Prussian Blue Coordination Polymers. Chem Mater. 2012;24:2698-2707.

8. Zhang C, Chen Z, Wang H, Nie Y, Yan J. Porous Fe_2O_3 Nanoparticles as Lithium-Ion Battery Anode Materials. ACS Appl. Nano Mater. 2021;4:8744-52.

9. Teng Y, Zhang XF, Xu TT, Deng ZP, Xu YM, Huo LH, et al. A spendable gas sensor with higher sensitivity and lowest detection limit towards H_2S: Porous α-Fe_2O_3 hierarchical tubule derived from poplar branch. Chem Eng J. 2020;392:123679.

10. Liu X, Chen K, Shim JJ, Huang J. Facile synthesis of porous Fe_2O_3 nanorods and their photocatalytic properties. J Saudi Chem Soc. 2015;19:479-84.

11. Krafft K.E., Wang C, Lin W, Metal-Organic Framework Templated Synthesis of Fe_2O_3/TiO_2 Nanocomposite for Hydrogen Production. Adv Mater. 2012;24:2014-2018.

12. Gao P, Liu R, Huang H, Jia X, Pan H, MOF-templated controllable synthesis of α-Fe_2O_3 porous nanorods and their gas sensing properties. RSC Adv. 2016;6:94699-705.

13. Li Y, Zhou YX, Ma X, Jiang HL. A metal–organic framework-templated synthesis of γ-Fe_2O_3 nanoparticles encapsulated in porous carbon for efficient and chemoselective hydrogenation of nitro compounds. Chem Commun. 2016;52:4199-4202.

14. Zhang L, Wu HB, Madhavi S, Hng HH, Lou XW. Formation of Fe_2O_3 Microboxes with Hierarchical Shell Structures from Metal–Organic Frameworks and Their Lithium Storage Properties. J Am Chem Soc. 2012;134(42):17388-91.

15. Zhang L, Wu HB, Xu R, Lou XW. Porous Fe_2O_3 nanocubes derived from MOFs for highly reversible lithium storage. CrystEngComm. 2013;15:9332.

16. Yao S, Zhang G, Zhang X, Zhao Y, Shi Z. Synthesis of α-Fe_2O_3 double-layer hollow spheres with carbon coating using carbonaceous sphere templates for lithium ion battery anodes. J Solid State Electrochem. 2021;25:267-278.

17. Wang S, Wang L, Yang T, Liu X, Zhang J, Zhu B, et al. Porous α-Fe_2O_3 hollow microspheres and their application for acetone sensor. J Solid State Chem. 2010;183:2869-76.

18. Nie Z, Wang Y, Zhang Y, Pan A. Multi-shelled α-Fe_2O_3 microspheres for high-rate supercapacitors. Sci China Mater. 2016;59:247-253.

19. Parajuli D, Tanaka H, Sakurai K, Hakuta Y, Kawamoto T. Thermal Decomposition Behavior of Prussian Blue in Various Conditions. Materials (Basel). 2021;14:1151.

20. Trinh LH, Khieu DQ, Long HT, Hoa TT, Quang DT, Cuong ND. A novel approach for synthesis of hierarchical mesoporous Nd_2O_3 nanomaterials. J. Rare Earths. 2017;35:677-82.

21. Son LL, Cuong ND, Thi TTV, Hieu LT, Trung DD, et al. Konjac glucomannan-templated synthesis of three-dimensional NiO nanostructures assembled from porous NiO nanoplates for gas sensors, RSC Adv. 2019;9:9584-93.

22. Li F, Zhang T, Gao X, Wang R, Li B. Coaxial electrospinning heterojunction SnO_2/Au-doped In_2O_3 core-shell nanofibers for acetone gas sensor. Sensors Actuators B Chem. 2017;252:822-30.

23. Li M, Li W, Liu S. Hydrothermal synthesis, characterization, and KOH activation of carbon spheres from glucose. Carbohydr Res. 2011;346:999-1004.

24. Nguyen TD. From formation mechanisms to synthetic methods toward shape-controlled oxide nanoparticles. Nanoscale. 2013;5:9455.